Benchmark solutions for sound propagation in an ideal wedge*

Luo Wen-Yu(骆文于)[a)†], Yang Chun-Mei(杨春梅)[a)b)], Qin Ji-Xing(秦继兴)[a)b)], and Zhang Ren-He(张仁和)[a)]

[a)] *State Key Laboratory of Acoustics, Institute of Acoustics, Chinese Academy of Sciences, Beijing* 100190, *China*
[b)] *University of Chinese Academy of Sciences, Beijing* 100049, *China*

(Received 21 August 2012; revised manuscript received 10 October 2012)

Sound propagation in a wedge-shaped waveguide with perfectly reflecting boundaries is one of the few range-dependent problems with an analytical solution, and hence provides an ideal benchmark for a full two-way solution to the wave equation. An analytical solution for the sound propagation in an ideal wedge with a pressure-release bottom was presented by Buckingham and Tolstoy [Buckingham and Tolstoy 1990 *J. Acoust. Soc. Am.* **87** 1511]. The ideal wedge problem with a rigid bottom is also of great importance in underwater acoustics. We present an analytical solution to the ideal wedge problem with a perfectly reflecting bottom, either rigid or pressure-release, which may be used to provide a means for investigating the sound field in depth-varying channels, and to establish the accuracy of numerical propagation models. Closed-form expressions for coupling matrices are also provided for the ideal waveguides characterized by a homogeneous water column bounded by perfectly reflecting boundaries. A comparison between the analytical solution and the numerical solution recently proposed by Luo *et al.* [Luo W Y, Yang C M and Zhang R H 2012 *Chin. Phys. Lett.* **29** 014302] is also presented, through which the accuracy of this numerical model is illustrated.

Keywords: coupled-mode theory, wedge-shaped waveguide, perfectly reflecting boundary, benchmark solution

PACS: 43.30.Bp, 43.30.Gv, 43.20.Fn **DOI:** 10.1088/1674-1056/22/5/054301

1. Introduction

Modeling sound propagation in range-dependent waveguides is of great interest in underwater acoustics. A number of approaches[1–7] have been developed for solving this problem over the past several decades, among which the normal mode method is very important. For problems characterized by a weak range-dependent variation, the mode coupling is negligible, and the adiabatic mode method proposed by Pierce[3] is sufficient. Otherwise, the mode coupling is significant and thus cannot be neglected. In recent years, advances in the coupled-mode method have been made by Fawcett,[8] Godin,[9] Abawi,[10] and Athanassoulis *et al.*[11] In those papers, additional terms are introduced in the series of local vertical normal modes to handle the inconsistency of these modes at nonhorizontal interfaces or bottom boundaries. An alternate approach, referred to as the stepwise coupled-mode method in the literature (see, e.g., Refs. [12]–[14]), is also an important means for treating range-dependent waveguide propagation. For instance, COUPLE is a widely used numerical model applying the stepwise coupled-mode method.[12,13] In that method, the range-dependent waveguide is represented by a sequence of range-independent stair steps and the coupled-mode solution is obtained by matching the solutions of the wave equations for neighboring segments at their common boundaries.

A stepwise coupled-mode method using the direct global matrix (DGM) approach was recently proposed by Luo *et al.*[15,16] This model is capable of addressing two-dimensional (2D) problems with either a point source in a cylindrical geometry or a line source in a plane geometry. Due to the use of the DGM approach, this method is numerically stable. In addition, by introducing appropriately normalized range solutions, the overflow problem inherent in certain existing models is entirely resolved. Moreover, the introduction of general source conditions enables this method to handle the scenario in which a line source is located right on the top of a sloping bottom. This numerical model is a full two-way model and hence is very accurate, which is established by comparing with the exact analytical solution to a benchmark problem proposed by the Acoustical Society of America (ASA).[16]

Analytical solutions to range-dependent waveguide problems are extremely useful for establishing the accuracy of numerical range-dependent propagation models. An analytical solution was proposed by Buckingham *et al.*[17] to solve a wedge problem involving a line source parallel to a wedge apex, a planar pressure-release sea surface, a planar pressure-release bottom, and a homogeneous water column supporting the acoustic field. That is a range-dependent problem with an exact analytical solution. Moreover, that problem is an ideal benchmark for a two-way numerical solution to the wave equation, in which the sound propagating to the apex will be completely backscattered due to the perfectly reflecting boundaries. However, it is difficult for certain numerical propagation models to handle a pressure-release bottom. Thus, an analyti-

*Project supported by the National Natural Science Foundation of China (Grant Nos. 11125420 and 10734100) and the Knowledge Innovation Program of the Chinese Academy of Sciences.

†Corresponding author. E-mail: lwy@mail.ioa.ac.cn

© 2013 Chinese Physical Society and IOP Publishing Ltd

cal solution to the wedge problem with a rigid bottom is also of great interest to the underwater acoustics community.

In this paper, we first present an analytical solution to the ideal wedge problem with a perfectly reflecting bottom, either rigid or pressure-release. Second, we give closed-form expressions for the coupling matrices for the propagation in a waveguide (not necessarily a wedge) bounded above by a pressure-release sea surface and below by a perfectly reflecting bottom. Third, we apply the numerical method presented in Refs. [15] and [16] to this wedge problem. A comparison between the analytical and the numerical solutions followed by a discussion is also provided.

2. Theory

The geometry of the ideal wedge problem is illustrated in Fig. 1, which involves a homogeneous water column and a line source parallel to the apex. A pressure-release sea surface and a rigid or pressure-release bottom constitute the boundaries of the wedge. A 2D cylindrical coordinate system with the origin at the apex is adopted in deriving the analytical solution. However, in the numerical model developed by Luo *et al.*,[15,16] a 2D Cartesian coordinate system is adopted instead.

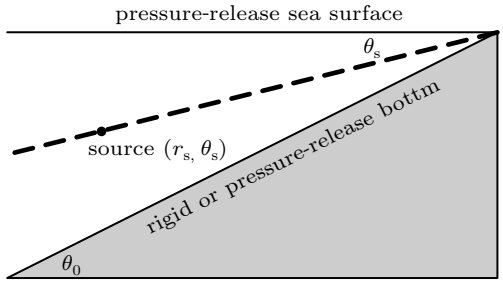


Fig. 1. Geometry of a wedge-shaped waveguide bounded above by a planar pressure-release sea surface and below by a planar rigid or pressure-release bottom. A line source is involved, which is parallel to the apex and located at (r_s, θ_s). The wedge angle is denoted by θ_0.

2.1. Analytical solution

In the cylindrical coordinates, the Helmholtz equation describing the wedge problem depicted in Fig. 1 is

$$\frac{1}{r}\frac{\partial}{\partial r}\left(r\frac{\partial p}{\partial r}\right)+\frac{1}{r^2}\frac{\partial^2 p}{\partial \theta^2}+k^2 p=-\frac{\delta(r-r_s)}{r}\delta(\theta-\theta_s), \quad (1)$$

where (r_s, θ_s) denotes the source location, and k is the wavenumber in water. The solution is presented as

$$p(r,\theta)=\sum_{n=1}^{\infty}\Theta_n(\theta)R_n(r). \quad (2)$$

By applying the separation of variables, together with the boundary conditions at the sea surface and at the bottom, we obtain the following analytical solution to the Helmholtz equation (1):

$$p(r,\theta)=\frac{\mathrm{i}\pi}{\theta_0}\sum_{n=1}^{\infty}\sin(\gamma_n\theta_s)\sin(\gamma_n\theta)\mathrm{J}_{\gamma_n}(kr_<)\mathrm{H}^{(1)}_{\gamma_n}(kr_>), \quad (3)$$

where θ_0 denotes the wedge angle, and J_{γ_n} and $\mathrm{H}^{(1)}_{\gamma_n}$ are Bessel and Hankel functions of the first kind of order γ_n, respectively, with

$$\gamma_n=\begin{cases}(n-1/2)\pi/\theta_0, & \text{rigid bottom},\\ n\pi/\theta_0, & \text{pressure-release bottom},\end{cases} \quad (4)$$

$$r_<=\min(r,r_s), \quad (5)$$

$$r_>=\max(r,r_s). \quad (6)$$

The detailed derivation is given in Appendix A.

Caution should be taken in evaluating the field solution in Eq. (3). When the order γ_n is much larger than the argument $kr_>$, although the product of $\mathrm{J}_{\gamma_n}(kr_<)\mathrm{H}^{(1)}_{\gamma_n}(kr_>)$ is bounded, the underflow problem may arise in evaluating $\mathrm{J}_{\gamma_n}(kr_<)$ and the overflow problem may arise in evaluating $\mathrm{H}^{(1)}_{\gamma_n}(kr_>)$. To avoid such numerical problems, the Debye asymptotic expansions[18] for large orders, which were used in Ref. [17] to handle the ideal wedge problem with a pressure-release bottom, are also used in this paper.

2.2. Numerical solution

A numerical model, referred to as DGMCM in this paper, for solving sound propagation in range-dependent waveguides was recently proposed by Luo *et al.*[15,16] This model has merits in terms of stability, accuracy, efficiency, and capability of addressing the scenario in which a line source is located right on the top of a sloping bottom. For completeness, here we briefly describe the formulation of this model. See Ref. [16] for details of the derivation.

In the formulation of this model, when dealing with a 2D problem involving a line source in a plane geometry, the Cartesian coordinates are introduced. The Helmholtz equation is

$$\frac{\partial^2 p}{\partial x^2}+\rho(z)\frac{\partial}{\partial z}\left(\frac{1}{\rho(z)}\frac{\partial p}{\partial z}\right)+\frac{\omega^2}{c^2(z)}p=-\delta(x-x_s)\delta(z-z_s), \quad (7)$$

where (x_s, z_s) denotes the source location.

We divide the range-dependent waveguide into a number of range-independent segments, and represent the field solution in segment j as

$$p^j(x,z)=\sum_{n=1}^{N}[a_n^j E_{1n}^j(x)+b_n^j E_{2n}^j(x)]\Psi_n^j(z), \quad (8)$$

where N is the total number of normal modes involved in mode coupling, a_n^j and b_n^j are modal amplitudes corresponding to the forward and the backward propagating waves, respectively, $\Psi_n^j(z)$ are the local vertical eigenfunctions, and $E_{1n}^j(x)$ and $E_{2n}^j(x)$ are normalized exponential functions defined respectively as

$$E_{1n}^j(x)=\exp[\mathrm{i}k_{xn}^j(x-x^{j-1})], \quad (9)$$

$$E_{2n}^j(x)=\exp[-\mathrm{i}k_{xn}^j(x-x^j)], \quad (10)$$

with k_{xn}^j denoting the horizontal wavenumbers. The solutions for $\boldsymbol{a}^j$ and $\boldsymbol{b}^j$, column vectors containing a_n^j and b_n^j with $n=1,2,\ldots,N$ in each segment, are obtained by solving the

following linear system of equations:

$$\boldsymbol{C}\boldsymbol{x} = \boldsymbol{v}, \tag{11}$$

where $\boldsymbol{x}$ is the column vector

$$\boldsymbol{x} = \left[\boldsymbol{b}^1\ \boldsymbol{a}^2\ \boldsymbol{b}^2\ \boldsymbol{a}^3\ \cdots\ \boldsymbol{b}^{j_s}\ \boldsymbol{a}^{j_s+1}\ \cdots\ \boldsymbol{b}^{J-1}\ \boldsymbol{a}^{J}\right]^{\mathrm{T}}, \tag{12}$$

$\boldsymbol{v}$ is the column vector

$$\boldsymbol{v} = \left[\boldsymbol{0}\ \boldsymbol{0}\ \boldsymbol{0}\ \boldsymbol{0}\ \cdots\ \boldsymbol{0}\ \boldsymbol{s}\ \cdots\ \boldsymbol{0}\ \boldsymbol{0}\right]^{\mathrm{T}}, \tag{13}$$

$\boldsymbol{s}$ is the column vector with entries

$$s_n = -\frac{\mathrm{i}}{\rho(z_{\mathrm{s}})}\frac{\Psi_n^{j_s}(z_{\mathrm{s}})}{k_{xn}^{j_s}}, \quad n = 1,2,\ldots,N, \tag{14}$$

and $\boldsymbol{C}$ is the global coefficient matrix

$$\boldsymbol{C} = \begin{bmatrix}
\widetilde{\boldsymbol{C}}^1 & -\boldsymbol{I} & -\boldsymbol{E}_2^2 & & & & & & \\
-\widehat{\boldsymbol{C}}^1 & -\boldsymbol{I} & \boldsymbol{E}_2^2 & & & & & & \\
 & \widetilde{\boldsymbol{C}}^2\boldsymbol{E}_1^2 & \widetilde{\boldsymbol{C}}^2 & -\boldsymbol{I} & -\boldsymbol{E}_2^3 & & & & \\
 & \widehat{\boldsymbol{C}}^2\boldsymbol{E}_1^2 & -\widehat{\boldsymbol{C}}^2 & -\boldsymbol{I} & \boldsymbol{E}_2^3 & & & & \\
 & & \ddots & \ddots & \ddots & \ddots & & & \\
 & & & \widetilde{\boldsymbol{C}}^{j_s}\boldsymbol{E}_1^{j_s} & \widetilde{\boldsymbol{C}}^{j_s} & -\boldsymbol{I} & -\boldsymbol{E}_2^{j_s+1} & & \\
 & & & \widehat{\boldsymbol{C}}^{j_s}\boldsymbol{E}_1^{j_s} & -\widehat{\boldsymbol{C}}^{j_s} & -\boldsymbol{I} & \boldsymbol{E}_2^{j_s+1} & & \\
 & & & & \ddots & \ddots & \ddots & \ddots & \\
 & & & & & \widetilde{\boldsymbol{C}}^{J-1}\boldsymbol{E}_1^{J-1} & \widetilde{\boldsymbol{C}}^{J-1} & -\boldsymbol{I} \\
 & & & & & \widehat{\boldsymbol{C}}^{J-1}\boldsymbol{E}_1^{J-1} & -\widehat{\boldsymbol{C}}^{J-1} & -\boldsymbol{I}
\end{bmatrix}. \tag{15}$$

Coupling matrices $\widetilde{\boldsymbol{C}}^j$ and $\widehat{\boldsymbol{C}}^j$ are respectively defined as

$$\widetilde{C}_{\nu n}^j = \int_0^\infty \frac{1}{\rho^{j+1}(z)}\Psi_\nu^{j+1}(z)\Psi_n^j(z)\,\mathrm{d}z, \tag{16}$$

$$\widehat{C}_{\nu n}^j = \frac{k_{xn}^j}{k_{x\nu}^{j+1}}\int_0^\infty \frac{1}{\rho^{j}(z)}\Psi_\nu^{j+1}(z)\Psi_n^j(z)\,\mathrm{d}z. \tag{17}$$

For an ideal waveguide involving a pressure-release surface, a rigid or pressure-release bottom, and a homogeneous water column, we have analytical modal solutions.[19] By substituting the analytical modal solutions into Eqs. (16) and (17), we obtain the following closed-form expressions for the coupling matrices.

The rigid-bottom case In this case, for upslope propagation, we have

$$\widetilde{C}_{\nu n}^j = FI, \tag{18}$$

$$\widehat{C}_{\nu n}^j = \frac{k_{xn}^j}{k_{x\nu}^{j+1}}F\left[I + (-1)^{\nu-1}\frac{2\cos(k_{zn}^j D^{j+1})}{k_{zn}^j}\right], \tag{19}$$

and for downslope propagation, we have

$$\widetilde{C}_{\nu n}^j = F\left[I + (-1)^{n-1}\frac{2\cos(k_{z\nu}^{j+1} D^{j})}{k_{z\nu}^{j+1}}\right], \tag{20}$$

$$\widehat{C}_{\nu n}^j = \frac{k_{xn}^j}{k_{x\nu}^{j+1}}FI. \tag{21}$$

The pressure-release-bottom case In this case, we have the following closed-form expressions for the coupling matrices:

$$\widetilde{C}_{\nu n}^j = FI, \tag{22}$$

$$\widehat{C}_{\nu n}^j = \frac{k_{xn}^j}{k_{x\nu}^{j+1}}FI. \tag{23}$$

Note that equations (22) and (23) apply for both upslope and downslope propagations in the case of a pressure-release bottom.

The notations in the above equations are defined as follows:

$$I = \begin{cases} \dfrac{\sin[(k_{z\nu}^{j+1} - k_{zn}^j)D]}{k_{z\nu}^{j+1} - k_{zn}^j} - \dfrac{\sin[(k_{z\nu}^{j+1} + k_{zn}^j)D]}{k_{z\nu}^{j+1} + k_{zn}^j}, & k_{z\nu}^{j+1} \neq k_{zn}^j, \\ D - \dfrac{\sin[(k_{z\nu}^{j+1} + k_{zn}^j)D]}{k_{z\nu}^{j+1} + k_{zn}^j}, & k_{z\nu}^{j+1} = k_{zn}^j, \end{cases} \tag{24}$$

$$F = (D^j D^{j+1})^{-1/2}, \tag{25}$$

$$D = \min(D^j, D^{j+1}), \tag{26}$$

with D^j and D^{j+1} denoting water depths in segments j and $j+1$, respectively. It is worth mentioning that the terms present only for the rigid-bottom case, that is, the term

$$(-1)^{\nu-1}\frac{2\cos(k_{zn}^j D^{j+1})}{k_{zn}^j} \tag{27}$$

in Eq. (19) and the term

$$(-1)^{n-1}\frac{2\cos(k_{z\nu}^{j+1} D^{j})}{k_{z\nu}^{j+1}} \tag{28}$$

in Eq. (20) arise from the nonzero contributions to the corresponding integrals in Eqs. (16) and (17) from the eigenfunctions below the water-bottom interface. However, the eigenfunctions remain zero below the water-bottom interface for the pressure-release-bottom case, resulting in the absence of such terms in the closed-form expressions for the coupling matrices in this case.

The model DGMCM differs from the model COUPLE in the following aspects. First, COUPLE converts the Helmholtz equation in a discretely range-dependent environment into a matrix two-point boundary value problem, and then solves it by applying the decoupling algorithm developed by Mattheij.[20] As described in Ref. [13], complicated and intensive operations on a great number of submatrices

are performed in COUPLE. However, by applying the DGM approach, the model DGMCM solves the global system of equations directly, resulting in great improvements in both numerical stability and efficiency. Second, the model DGMCM uses normalized range solutions different from those in COUPLE, which entirely resolves the overflow problem inherent in COUPLE. Third, the model DGMCM implements the source conditions recently proposed by Luo *et al*.[15] As a result, this model has the ability to deal with the scenario in which a line source is located inside the range-dependent region, for instance, on the top of a slope. Finally, for problems with perfectly reflecting boundaries (a pressure-release surface and a pressure-release or rigid bottom) as well as for a homogeneous water column, closed-form expressions for the coupling matrices are implemented in DGMCM, yielding significant improvements in both accuracy and efficiency.

In this paper, the field results are shown in terms of transmission loss (TL) in units of dB re 1 m, which is defined as

$$\mathrm{TL} = -20\log_{10}\left|\frac{p(\boldsymbol{r})}{p_0(1)}\right|, \tag{29}$$

where $\boldsymbol{r}$ is the location of a field point, and the reference pressure takes the following form:

$$p_0(x) = \frac{\mathrm{i}}{4}\mathrm{H}_0^{(1)}(k_0 x). \tag{30}$$

Here, k_0 denotes the reference wavenumber defined as $k_0 = 2\pi f/1500$, with f denoting the source frequency.

Note that although DGMCM is applied to a line source problem in this paper, this model has the ability to address the point source problem too, see Ref. [16] for details.

3. Numerical examples

Below we first give a brief description of the ideal wedge problem, followed by results for this problem with different bottom types and slope angles. Finally, a discussion is provided.

3.1. Problem description

Consider the wedge-shaped waveguide illustrated in Fig. 2. The environment consists of a homogeneous water column with sound speed $c_\mathrm{w} = 1500$ m/s and density $\rho_\mathrm{w} = 1.0$ g/cm^3, bounded by plane, perfectly reflecting boundaries, and the line source is parallel to the apex. The wedge angle is approximately 2.86°. The source is located at 100 m in depth and 4.0 km in range, and the source frequency is 25 Hz. The considered receiver depth is 30 m. The ideal wedge problem involving a pressure-release bottom is one of the three range-dependent benchmark problems posed and discussed at two consecutive meetings of the Acoustical Society of America.[21,22] A detailed discussion of the numerical solutions to this problem can be found in Ref. [23]. In this paper, two types of bottom boundary conditions are considered: rigid and pressure-release. Since the sound propagating towards the wedge apex will be completely backscattered due to the perfectly reflecting boundaries, this test problem is an ideal benchmark for a full two-way solution of the wave equation.

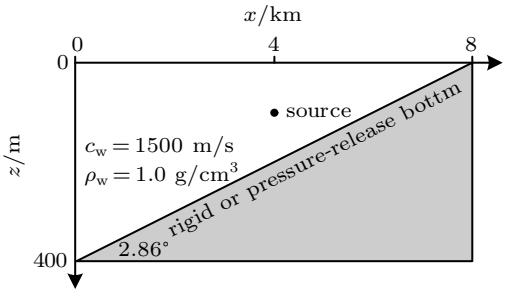


Fig. 2. Schematic diagram of the wedge-shaped waveguide environment used in the numerical examples. A line source is located at 100-m depth and 4-km range. The source frequency is 25 Hz.

3.2. Results for the wedge problem with a pressure-release bottom

Consider the problem depicted in Fig. 2 involving a pressure-release bottom. Although the waveguide at the source range can support 6 horizontally propagating modes, only the odd-numbered modes, that is, modes 1, 3, and 5, are excited with the source located at mid-depth. Note that in order to obtain convergent results, in general, a number of evanescent modes should be involved in mode coupling. For this problem, a convergence analysis shows that a total number of 20 normal modes is sufficient to reach convergence. In addition, the slope is divided into 1200 segments for DGMCM. A comparison of the field results obtained by the analytical solution and the numerical model DGMCM is provided in Fig. 3, which shows excellent overall agreement. The positions of the peaks and troughs are the same, and the absolute levels of the curves are also in good agreement within a fraction of 1 dB. Since the ideal wedge problem is a particularly stringent test for numerical propagation models, the excellent agreement indicates that this recently developed coupled-mode model is very accurate.

In addition, the mode stripping effect is evident in Figs. 3(c) and 3(d) in the upslope region, that is, from 4 km to 8 km in range. As is known, only the odd-numbered modes, i.e., modes 1, 3, and 5, are excited by the source. These three modes propagate upslope towards the wedge apex until mode 5 first reaches its critical depth and is turned around followed by modes 3 and 1, which reach their critical depths further upslope. No energy propagates beyond the critical depth for mode 1. It can be shown that the critical depths are determined by

$$D_n = n\frac{\lambda}{2}, \quad n = 1, 2, \ldots, \tag{31}$$

in an ideal waveguide involving a pressure-release bottom. For the wedge problem shown in Fig. 2, the critical range of mode n is determined by

$$x_n = 8 - D_n/50. \tag{32}$$

Thus, we obtain the critical depths and the associated critical ranges for modes 1–6 as shown in Table 1. The critical ranges for the first 6 modes are also indicated by the white dashed lines in Figs. 3(c) and 3(d). Note that no mode stripping effect occurs for modes 2, 4, and 6 because these modes are not excited by the source.

Table 1. Critical depths and associated critical ranges for the first 6 modes in the pressure-release bottom case.

Mode	Critical depth/m	Critical range/km
1	30	7.4
2	60	6.8
3	90	6.2
4	120	5.6
5	150	5.0
6	180	4.4

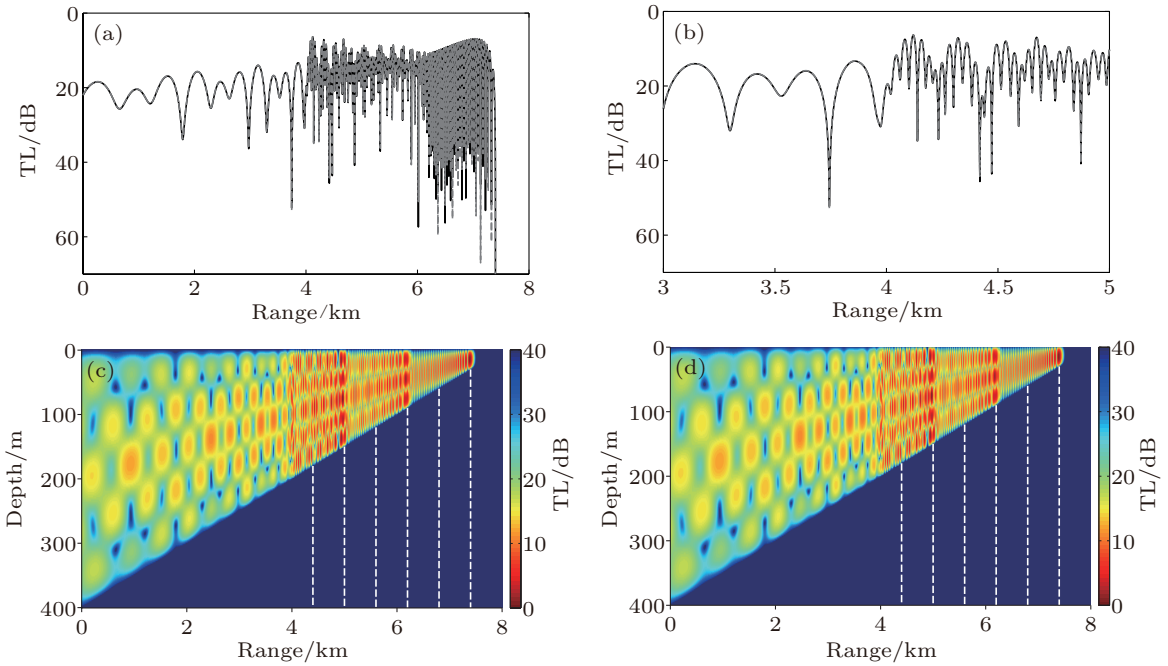


Fig. 3. Comparison between the analytical solution and DGMCM for the wedge problem with a pressure-release bottom. (a) TL at 30-m depth from 0 km to 8 km in range; (b) TL at 30-m depth from 3 km to 5 km in range; (c) TL versus range and depth in the analytical solution; (d) TL versus range and depth in DGMCM. In panels (a) and (b), the black solid line is the analytical solution and the gray dashed line is the DGMCM result. In panels (c) and (d), the white dashed lines indicate the critical ranges of modes 1–6 from right to left.

It is also interesting to observe rapid spatial fluctuations in the range from 4 km to 8 km from Fig. 3, in contrast to the slowly oscillating structure in the range from 0 km to 4 km. The physical interpretation is that between 4 km and 8 km, for each mode, the outgoing and the incoming waves are comparable in intensity, leading to the rapidly oscillating interference structure in the transmission loss. However, between 0 km and 4 km, the outgoing wave is dominant and the incoming wave is negligible, resulting in the slowly oscillating structure shown in Fig. 3.

3.3. Results for the wedge problem with a rigid bottom

Consider the problem depicted in Fig. 2 involving a rigid bottom. In numerical implementations of both the analytical solution and DGMCM, a total of 20 modes are used. In this problem, the waveguide at the source range can support 7 horizontally propagating modes, all of which are excited by the source. Moreover, the slope is represented by 1200 segments for DGMCM. A comparison of the field results obtained by the analytical solution and DGMCM is given in Fig. 4, which shows good agreement between these two methods.

Table 2. Critical depths and associated critical ranges for the first 7 modes in the rigid bottom case.

Mode	Critical depth/m	Critical range/km
1	15	7.7
2	45	7.1
3	75	6.5
4	105	5.9
5	135	5.3
6	165	4.7
7	195	4.1

Like the case involving a pressure-release bottom, the mode stripping effect also occurs in this rigid-bottom case, as is evident in Figs. 4(c) and 4(d). In this case, the critical depths

are determined by

$$D_n = \left(n - \frac{1}{2}\right)\frac{\lambda}{2}, \quad n = 1, 2, \ldots \tag{33}$$

For the problem considered here, 7 horizontally propagating modes are excited by the source, and propagate upslope until they reach their critical depths and are turned around one by one. We obtain with Eqs. (33) and (32) the critical depths and the associated critical ranges, as shown in Table 2. The critical ranges for the first 7 modes are also indicated by the white dashed lines in Figs. 4(c) and 4(d). In addition, the rapidly oscillating interference structure between the outgoing and the incoming waves from 4 km to 8 km in range is evident in Fig. 4, just like that observed in Fig. 3 for the pressure-release-bottom case.

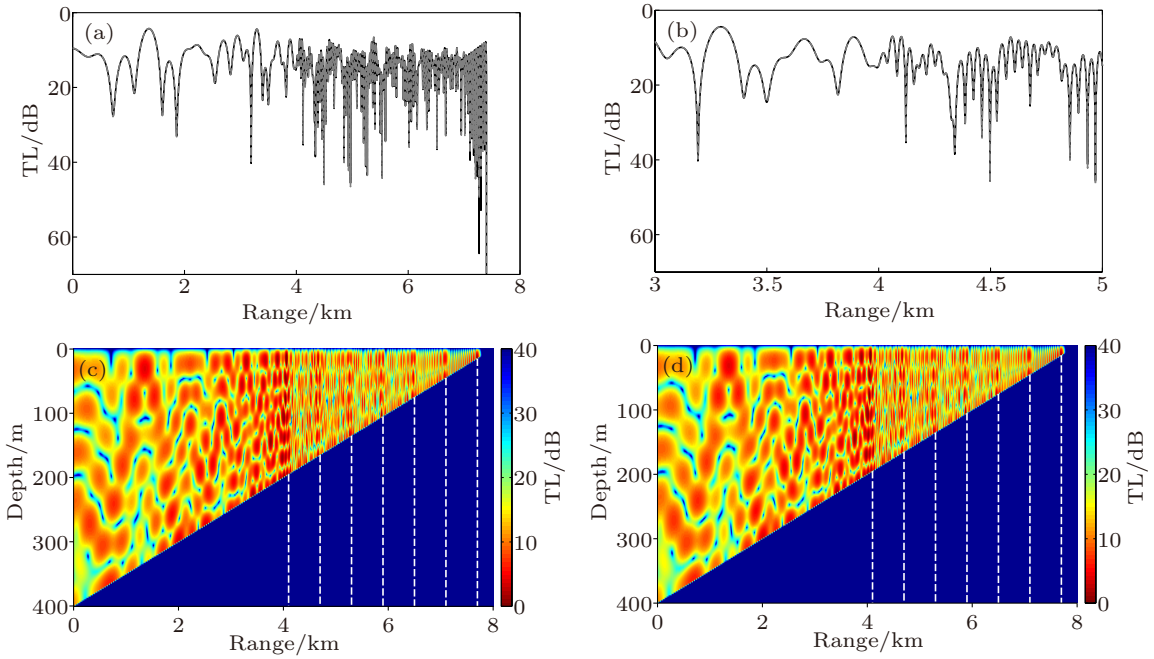


Fig. 4. Comparison between the analytical solution and DGMCM for the wedge problem with a rigid bottom. (a) TL at 30-m depth from 0 km to 8 km in range; (b) TL at 30-m depth from 3 km to 5 km in range; (c) TL versus range and depth in the analytical solution; (d) TL versus range and depth in DGMCM. In panels (a) and (b), the black solid line is the analytical solution and the gray dashed line is the DGMCM result. In panels (c) and (d), the white dashed lines indicate the critical ranges of modes 1–7 from right to left.

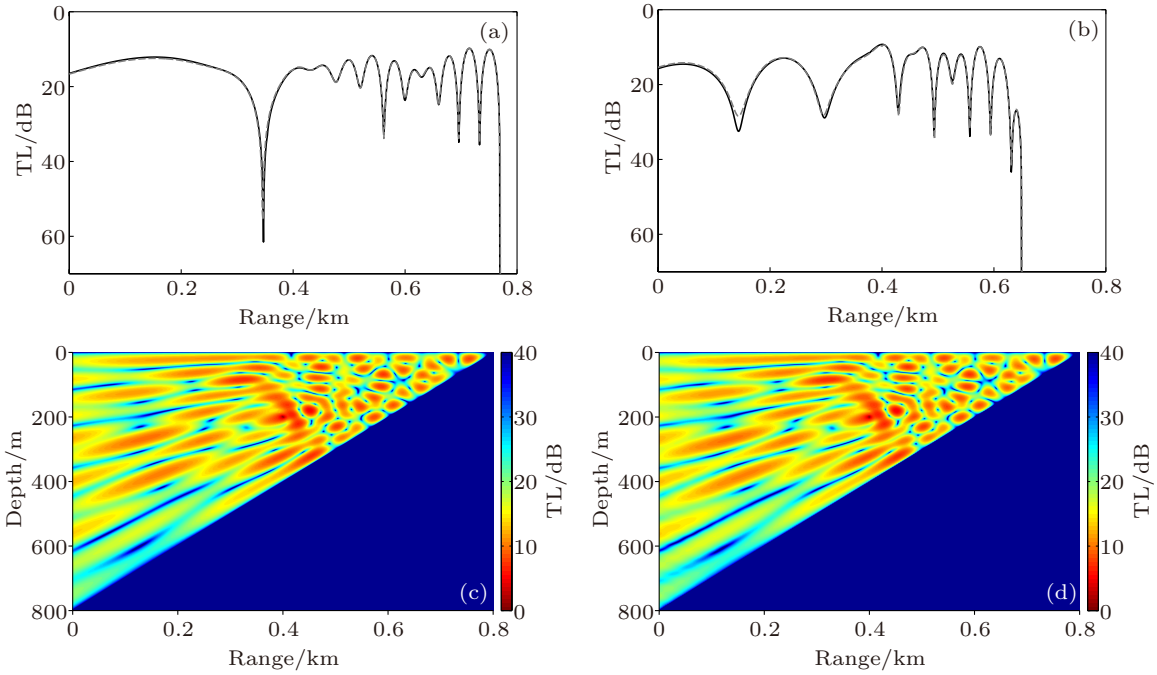


Fig. 5. Comparison between the analytical solution and DGMCM for the pressure-release-bottom case with the slope angle of 45°. (a) TL at 30-m depth; (b) TL at 150-m depth; (c) TL versus range and depth in the analytical solution; (d) TL versus range and depth in DGMCM. In panels (a) and (b), the black solid line is the analytical solution and the gray dashed line is the DGMCM result.

3.4. Results for the wedge problem with a large slope angle

Theoretically, the exact analytical solution given in Section 2.1 and the numerical solution given in Section 2.2 are valid for the ideal wedge problem with an arbitrary slope angle at any frequency. Here we consider an ideal wedge problem with a slope angle of 45°, which is much larger than that in the ASA benchmark problem. In this problem, the initial water depth is 800 m, which decreases linearly to 0 m in the range interval from 0 km to 0.8 km, and hence the slope angle is 45°. The line source is located at 200 m in depth and 0.4 km in range, and the source frequency is 25 Hz. A perfectly reflecting bottom (rigid or pressure-release) is considered. In the numerical implementations of both the analytical solution and DGMCM, a total of 60 modes are used. Moreover, the slope is represented by 600 segments for DGMCM. Comparisons of the results by the analytical solution and the numerical model DGMCM are shown in Fig. 5 for the pressure-release-bottom case and Fig. 6 for the rigid-bottom case, both of which show excellent agreement between these two methods, indicating that the proposed analytical solution and DGMCM are still valid for large slope angles. Furthermore, note that with the proposed closed-form expressions for the coupling matrices, DGMCM can be applied to general range-dependent waveguides characterized by a homogeneous water column and perfectly reflecting boundaries, not necessarily ideal wedges.

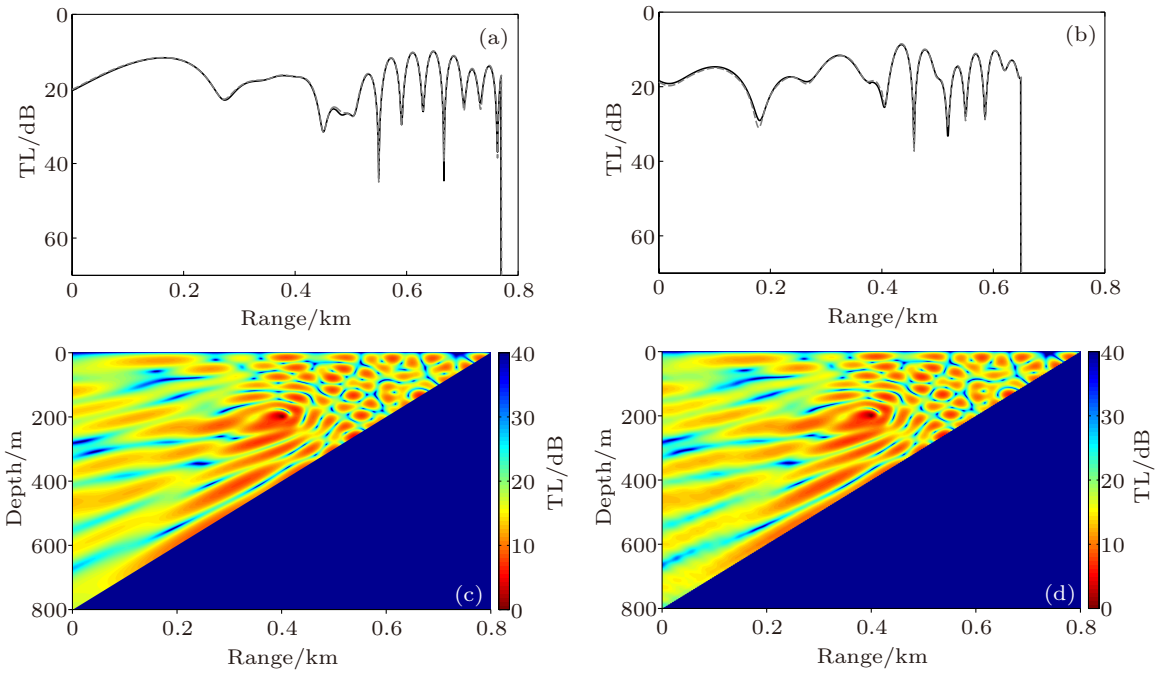


Fig. 6. Comparison between the analytical solution and DGMCM for the rigid-bottom case with the slope angle of 45°. (a) TL at 30-m depth; (b) TL at 150-m depth; (c) TL versus range and depth in the analytical solution; (d) TL versus range and depth in DGMCM. In panels (a) and (b), the black solid line is the analytical solution and the gray dashed line is the DGMCM result.

3.5. Discussion

Theoretically, as also confirmed by numerical simulations, the proposed analytical solution for sound propagation in ideal wedges is valid for any frequency and any slope angle. Note that with the use of the proposed closed-form expressions for the coupling matrices, the numerical model DGMCM can be applied to general range-dependent waveguides characterized by a homogeneous water column, a pressure-release surface, and a rigid or pressure-release bottom, not necessarily wedge-shaped waveguides. Moreover, this model can be easily generalized to more realistic waveguides. For this purpose, a numerical normal mode model such as KRAKEN[24] should be adopted to provide local modal solutions and their associated coupling matrices.

In addition, it is worth noting that for the coupled-mode approaches developed by Fawcett,[8] Godin,[9] and Athanassoulis *et al.*,[11] special treatments were taken regarding the boundary condition at the bottom. In the formulations of those papers, the series of standard local vertical modes converges very slowly, since at a rigid bottom (or at a penetrable interface) these modes satisfy an incorrect Neumann boundary condition, wherein the normal derivative operator $\partial/\partial n$ is replaced by the derivative $\partial/\partial z$ in the vertical direction. To solve this problem, additional terms have been introduced in the series. However, this problem does not exist in the stepwise coupled-mode method, where the waveguide is range-independent in each segment. This is verified by the numerical results shown in this paper, where excellent agreement

between the analytical solution and the numerical stepwise coupled-mode model is observed.

4. Conclusion

In this paper, an exact analytical solution for the sound propagation in an ideal wedge is proposed, which can be used as a primary range-dependent benchmark to establish the accuracy of numerical models. A detailed derivation of the exact analytical solution is also provided. In addition, closed-form expressions for the coupling matrices for the ideal waveguides are given and applied in a recently developed numerical stepwise coupled-mode model, DGMCM, for addressing the problem of sound propagation in an ideal wedge. The proposed closed-form expressions for the coupling matrices can be applied to general ideal waveguides (not necessarily wedges) characterized by a homogeneous water column, a pressure-release sea surface, and a rigid or pressure-release bottom. The results obtained by the analytical solution and DGMCM are in excellent agreement, indicating that the later can serve as a secondary range-dependent benchmark. Furthermore, physical phenomena such as interference between outgoing and incoming waves and the mode stripping effect are also analyzed.

Note that the proposed exact analytical solution and the numerical model using the closed-form coupling matrices are valid only for the ideal wedge problem which involves a homogeneous water column, a pressure-release surface, a rigid or pressure-release bottom, and a line source parallel to the wedge apex. They cannot be used to analyze certain physical phenomena such as horizontal refraction and interaction between normal modes of discrete and continuous spectra which are common for sound propagation in a continental shelf environment in reality. Despite of such limitations, the proposed analytical solution and the numerical model developed in Refs. [15] and [16] can find useful applications in underwater acoustics, especially, to check and evaluate other numerical propagation models when the coupling between discrete normal modes is strong but the horizontal refraction and coupling to the continuous spectrum is negligible.

In summary, an analytical solution to the ideal wedge problem involving a pressure-release sea surface, a rigid or pressure-release bottom, a homogeneous water column, and a line source parallel to the wedge apex is proposed, which is extremely useful as a primary range-dependent benchmark. Because it provides exact solutions, it may be used to establish the accuracy of numerical propagation models. In addition, a recently developed stepwise coupled-mode model[15,16] is applied to this ideal wedge problem. Closed-form expressions for the coupling matrices for propagation in waveguides bounded above by a pressure-release sea surface and below by a rigid or pressure-release bottom are also given. The excellent agreement between the analytical solution and the numerical model establishes the accuracy of the latter. Consequently, this numerical model can serve as a secondary benchmark against other numerical models, especially when addressing range-dependent waveguide propagation problems without exact analytical solutions.

Appendix A: Derivation of the analytical solution for the ideal wedge problem

In the cylindrical coordinates, the Helmholtz equation describing the wedge problem illustrated in Fig. 1 is

$$\frac{1}{r}\frac{\partial}{\partial r}\left(r\frac{\partial p}{\partial r}\right)+\frac{1}{r^2}\frac{\partial^2 p}{\partial \theta^2}+k^2 p=-\frac{\delta(r-r_{\rm s})}{r}\delta(\theta-\theta_{\rm s}), \quad \text{(A1)}$$

where $(r_{\rm s},\theta_{\rm s})$ denotes the source location. Represent the solution in the form

$$p(r,\theta)=\sum_{n=1}^{\infty}\Theta_n(\theta)R_n(r). \quad \text{(A2)}$$

Substituting Eq. (A2) into the homogeneous Helmholtz equation, we obtain

$$\frac{1}{r}\frac{\mathrm{d}}{\mathrm{d}r}\left(r\frac{\mathrm{d}R_n}{\mathrm{d}r}\right)\Theta_n+\frac{1}{r^2}R_n\frac{\mathrm{d}^2\Theta_n}{\mathrm{d}\theta^2}+k^2\Theta_n R_n=0, \quad \text{(A3)}$$

or equivalently,

$$\frac{r}{R_n}\frac{\mathrm{d}}{\mathrm{d}r}\left(r\frac{\mathrm{d}R_n}{\mathrm{d}r}\right)+\frac{1}{\Theta_n}\frac{\mathrm{d}^2\Theta_n}{\mathrm{d}\theta^2}+k^2r^2=0. \quad \text{(A4)}$$

Apply the separation of variables, and let

$$\frac{1}{\Theta_n}\frac{\mathrm{d}^2\Theta_n}{\mathrm{d}\theta^2}=-\gamma_n^2, \quad \text{(A5)}$$

$$\frac{r}{R_n}\frac{\mathrm{d}}{\mathrm{d}r}\left(r\frac{\mathrm{d}R_n}{\mathrm{d}r}\right)+k^2r^2=\gamma_n^2, \quad \text{(A6)}$$

with γ_n denoting the separation constant. From Eq. (A5), we obtain the solution for $\Theta_n(\theta)$

$$\Theta_n(\theta)=A_n\sin(\gamma_n\theta)+B_n\cos(\gamma_n\theta), \quad \text{(A7)}$$

where A_n and B_n are constants to be determined by the boundary conditions. Impose the boundary condition at the sea surface

$$\Theta_n(0)=0, \quad \text{(A8)}$$

we obtain

$$B_n=0. \quad \text{(A9)}$$

For the case of a rigid bottom, the boundary condition at the bottom

$$\frac{\mathrm{d}\Theta_n}{\mathrm{d}\theta}|_{\theta_0}=0 \quad \text{(A10)}$$

yields

$$\gamma_n=\left(n-\frac{1}{2}\right)\frac{\pi}{\theta_0}, \quad n=1,2,\ldots \quad \text{(A11)}$$

Whereas for the case of a pressure-release bottom, the boundary condition at the bottom

$$\Theta_n(\theta_0)=0, \quad \text{(A12)}$$

yields

$$\gamma_n = n\frac{\pi}{\theta_0}, \quad n = 1, 2, \ldots \tag{A13}$$

The coefficient A_n can be obtained by applying the orthonormality relation

$$\int_0^{\theta_0} \Theta_n(\theta)\Theta_m(\theta)\mathrm{d}\theta = \delta_{nm}, \tag{A14}$$

which yields

$$A_n = \sqrt{\frac{2}{\theta_0}}. \tag{A15}$$

Therefore, the solution for $\Theta_n(\theta)$ is obtained as

$$\Theta_n(\theta) = \sqrt{\frac{2}{\theta_0}}\sin(\gamma_n\theta), \tag{A16}$$

where

$$\gamma_n = \begin{cases} \left(n - 1/2\right)\pi/\theta_0, & \text{rigid bottom,} \\ n\pi/\theta_0, & \text{pressure-release bottom.} \end{cases} \tag{A17}$$

Next, we continue to solve for $R_n(r)$. Substituting Eqs. (A2) and (A5) into Eq. (A1), we obtain

$$\sum_{n=1}^{\infty}\left[\frac{1}{r}\frac{\mathrm{d}}{\mathrm{d}r}\left(r\frac{\mathrm{d}R_n}{\mathrm{d}r}\right) - \frac{R_n}{r^2}\gamma_n^2\Theta_n R_n + k^2\Theta_n R_n\right] = -\frac{\delta(r-r_\mathrm{s})}{r}\delta(\theta-\theta_\mathrm{s}). \tag{A18}$$

Apply the operator

$$\int_0^{\theta_0}(\cdot)\Theta_m\,\mathrm{d}\theta, \tag{A19}$$

we obtain

$$\frac{1}{r}\frac{\mathrm{d}}{\mathrm{d}r}\left(r\frac{\mathrm{d}R_n}{\mathrm{d}r}\right) + \left(k^2 - \frac{\gamma_n^2}{r^2}\right)R_n = -\frac{\delta(r-r_\mathrm{s})}{r}\Theta_n(\theta_\mathrm{s}). \tag{A20}$$

Rewrite Eq. (A20) as

$$\frac{1}{r}\frac{\mathrm{d}}{\mathrm{d}r}\left\{r\frac{\mathrm{d}[R_n/\Theta_n(\theta_\mathrm{s})]}{\mathrm{d}r}\right\} + \left(k^2 - \frac{\gamma_n^2}{r^2}\right)\frac{R_n}{\Theta_n(\theta_\mathrm{s})} = -\frac{\delta(r-r_\mathrm{s})}{r}, \tag{A21}$$

which is a Bessel equation and has the solution

$$\frac{R_n}{\Theta_n(\theta_\mathrm{s})} = \mathrm{i}\frac{\pi}{2}\mathrm{J}_{\gamma_n}(kr_<)\mathrm{H}^{(1)}_{\gamma_n}(kr_>). \tag{A22}$$

Here, J_{γ_n} and $\mathrm{H}^{(1)}_{\gamma_n}$ are Bessel and Hankel functions of the first kind of order γ_n, respectively, and $r_<$ and $r_>$ are defined as follows:

$$r_< = \min(r, r_\mathrm{s}), \tag{A23}$$

$$r_> = \max(r, r_\mathrm{s}). \tag{A24}$$

Thus, we obtain the solution for $R_n(r)$

$$R_n(r) = \mathrm{i}\frac{\pi}{2}\Theta_n(\theta_\mathrm{s})\mathrm{J}_{\gamma_n}(kr_<)\mathrm{H}^{(1)}_{\gamma_n}(kr_>). \tag{A25}$$

Substitution of Eqs. (A16) and (A25) into Eq. (A2) yields the solution to Eq. (A1)

$$p(r,\theta) = \mathrm{i}\frac{\pi}{\theta_0}\sum_{n=1}^{\infty}\sin(\gamma_n\theta)\sin(\gamma_n\theta_\mathrm{s})\mathrm{J}_{\gamma_n}(kr_<)\mathrm{H}^{(1)}_{\gamma_n}(kr_>), \tag{A26}$$

where γ_n is given in Eq. (A17).

References

[1] Collis J M, Siegmann W L, Jensen F B, Zampolli M, Küsel E T and Collins M D 2008 *J. Acoust. Soc. Am.* **123** 51
[2] Thompson L L 2006 *J. Acoust. Soc. Am.* **119** 1315
[3] Pierce A D 1965 *J. Acoust. Soc. Am.* **37** 19
[4] Porter M B, Jensen F B and Ferla C M 1991 *J. Acoust. Soc. Am.* **89** 1058
[5] Wang H Z, Wang N and Gao D Z 2012 *J. Acoust. Soc. Am.* **131** 1047
[6] Gao B, Yang S E, Piao S C and Huang Y W 2010 *Sci. China-Phys. Mech. Astron.* **53** 2216
[7] Luo W Y and Schmidt H 2009 *J. Acoust. Soc. Am.* **125** 52
[8] Fawcett J A 1992 *J. Acoust. Soc. Am.* **92** 290
[9] Godin O A 1998 *J. Acoust. Soc. Am.* **103** 159
[10] Abawi A T 2002 *J. Acoust. Soc. Am.* **111** 160
[11] Athanassoulis G A, Belibassakis K A, Mitsoudis D A, Kampanis N A and Dougalis V A 2008 *J. Comp. Acoustics* **16** 83
[12] Evans R B 1983 *J. Acoust. Soc. Am.* **74** 188
[13] Evans R B 1986 *J. Acoust. Soc. Am.* **80** 1414
[14] Abawi A T, Kuperman W A and Collins M D 1997 *J. Acoust. Soc. Am.* **102** 233
[15] Luo W Y, Yang C M and Zhang R H 2012 *Chin. Phys. Lett.* **29** 014302
[16] Luo W Y, Yang C M, Qin J X and Zhang R H 2012 *Sci. China G: Phys. Mech. Astron.* **55** 572
[17] Buckingham M J and Tolstoy A 1990 *J. Acoust. Soc. Am.* **87** 1511
[18] Abramowitz M and Stegun I A 1972 *Handbook of Mathematical Functions with Formulas, Graphs, and Mathematical Tables* (Washington DC: National Bureau of Standards) pp. 366–367
[19] Jensen F B, Kuperman W A, Porter M B and Schmidt H 2011 *Computational Ocean Acoustics* (2nd edn.) (New York: Springer) pp. 344–349
[20] Mattheij R M M 1985 *SIAM Rev.* **27** 1
[21] Felsen L B 1986 *J. Acoust. Soc. Am.* (Suppl. 1) **80** S36
[22] Felsen L B 1987 *J. Acoust. Soc. Am.* (Suppl. 1) **81** S39
[23] Jensen F B and Ferla C M 1990 *J. Acoust. Soc. Am.* **87** 1499
[24] Porter M B 1991 *The KRAKEN Normal Mode Program* (Technical Report No. SM-245) (La Spezia: SACLANT Undersea Research Center)